



HAL
open science

Defining conditions for bulking and debulking in lahars

Emma E. Doyle, Shane J. Cronin, Jean-Claude Thouret

► **To cite this version:**

Emma E. Doyle, Shane J. Cronin, Jean-Claude Thouret. Defining conditions for bulking and debulking in lahars. Geological Society of America Bulletin, 2011, 123 (7-8), pp.1234-1246. 10.1130/B30227.1 . hal-00682723

HAL Id: hal-00682723

<https://hal.science/hal-00682723v1>

Submitted on 12 Nov 2024

HAL is a multi-disciplinary open access archive for the deposit and dissemination of scientific research documents, whether they are published or not. The documents may come from teaching and research institutions in France or abroad, or from public or private research centers.

L'archive ouverte pluridisciplinaire **HAL**, est destinée au dépôt et à la diffusion de documents scientifiques de niveau recherche, publiés ou non, émanant des établissements d'enseignement et de recherche français ou étrangers, des laboratoires publics ou privés.

Defining conditions for bulking and debulking in lahars

E.E. Doyle^{1†}, S.J. Cronin², and J.-C. Thouret³

¹Joint Centre for Disaster Research, Massey University, P.O. Box 756, Wellington 6140, New Zealand

²Institute of Natural Resources, Massey University, Private Bag 11 222, Palmerston North 4442, New Zealand

³Laboratoire Magmas et Volcans UMR 6524, Centre National de la Recherche Scientifique (CNRS), Université Blaise Pascal, Observatoire de Physique de Globe at Clermont-Ferrand (OPGC) et Institute of Research and Development (IRD), 5 rue Kessler, 63038 Clermont-Ferrand cedex, France

ABSTRACT

Through measurements at Semeru Volcano, East Java, we define the conditions under which bulking (entrainment of sediment and pore water) and debulking (dilution and sedimentation) occur in rain-triggered volcanic floods (lahars). Two observation sites were installed 510 m apart, along the Curah Leng-kong River, 11.5 km southeast of Semeru's summit. This 30-m-wide box valley, with a gravel and lava base, represents a real-world flume analogy. Pore-pressure sensors provided stage measurements, a broad-band seismograph gave insight into sediment content and frictional-collisional behavior, video cameras were used to measure surface velocities, and direct bucket samples were taken. Eight rainfall-induced lahars were recorded, lasting 1–3 h with heights of 0.5–2 m, peak velocities of 3–7 m/s, and discharges of 25–250 m³/s. Flows ranged from typical (<40 wt% sediment) to coarse and dense hyperconcentrated flows (50–60 wt% sediment). Multiple distinct flow “packets” occurred within the complex lahars, and were used to determine internal changes between sites. From the multiparameter data set at each site, volumetric bulking and wave shortening, due to portions of the lahar accelerating toward the flow front, are identified. Initial debulking of lahars between sites may reflect drainage into the dry substrate. Estimates of discharge and volume at each site lead to the quantification of bulking and debulking by these actively flowing lahars along the channel reach. From this, we observe that bulking can be localized to certain parts of lahars, resulting in intraevent increases in peak discharge that are greater than what would occur if bulking was evenly distributed throughout the flow. Such data are essential for the development of numerical descriptions and hazard models for mass flows.

INTRODUCTION

Lahars are one of the most hazardous phenomena associated with volcanoes. These sediment-water, gravity-driven flows are characterized by high velocities, large impact forces, and long runouts. They cause major loss of human life, destruction of property, water supplies, and infrastructure, and burial of agricultural land, roads, and livestock (see Jakob and Hungr, 2005). During the twentieth century alone, lahars have caused an estimated 30,734 fatalities (Witham, 2005), second only to pyroclastic density currents (44,928) for all volcanic hazards. They are commonly defined as a “rapidly flowing mixture of rock debris and water (other than normal streamflow) from a volcano” (Smith and Fritz, 1989).

Lahars can originate from a wide range of processes, including crater-lake outbreaks, eruption-induced melting of snow, rain-induced remobilization of loose volcanic sediment, and transformation of debris avalanches downvalley. They often begin as erosive watery floods that entrain sediment and water, transforming into sand-dominated, hyperconcentrated flows and extremely coarse and sediment-rich debris flows. The volume and discharge of these flows can increase by several times downstream during transformation, where erosion, bulking, and sedimentation are thought to control the dominant flow phase (Scott, 1988; Scott et al., 1995). The total volume of the flow is controlled by the efficiency of entrainment (Hungr et al., 2005). Predictive models of lahar routing and inundation are vital tools for the identification of hazard zones and the development of hazard mitigation structures. Validation, verification, and development of these models requires an accurate and detailed determination of lahar flow characteristics and evolution, and an understanding of the fundamental controls on flow-behavior changes. However, due to their sudden onset and the dangers involved, scientific observations of active lahars are scarce, and thus

these highly hazardous flows remain a poorly understood phenomenon.

Existing observations of lahars in motion include those of anticipated outbreak lahars (e.g., Cronin et al., 1999; Manville et al., 2007), and rain-triggered mass flows that occur in tropical volcanic areas (e.g., Lavigne and Thouret, 2002), alpine regions (e.g., Arattano and Moia, 1999; Lenzi and Marchi, 2000), or flash-flood prone areas (Pierson and Scott, 1985; Xu, 2002). In addition, investigations of artificial flume experiments provide further understanding of how confinement, water concentration, slope angle, and grain-size distribution can affect the flow runout, velocity, and deposit morphology (e.g., Iverson, 1997; Iverson et al., 1997; Major, 1997). Frequent rainfall-induced lahars provide a valuable opportunity to investigate these parameters for real-world flows in natural open channels. At Semeru Volcano, East Java, the Curah Leng-kong channel has been utilized since 2002 as a safe lahar observation site (Thouret et al., 2007). Since 1967, this volcano produces daily Vulcanian explosions, with larger scale events leading to pyroclastic flows occurring every one to seven years (Lavigne and Suwa, 2004). Consequently, the volcano flanks are covered by abundant, unconsolidated, and fresh clastic debris available for erosion and mobilization (Fig. 1). Annual rainfall between 2000 and 3700 mm triggers a high number of rainfall-induced lahars (Lavigne and Suwa, 2004; Dumaisnil et al., 2010). In the peak rainy season of January to April, these can be produced on a daily to weekly basis, which is ideal for geophysical observations.

During a three-week period in February and March 2008, we recorded a total of eight lahars at Semeru Volcano (Doyle et al., 2009, 2010; Dumaisnil et al., 2010, and General Characteristics of Recorded Flows to Date, below). Doyle et al. (2009, 2010) have demonstrated that by using two closely located instrument sites (510 m apart) distinct arrivals within the lahars can be traced downstream, and the shortening

[†]E-mail: emmadoyle79@gmail.com

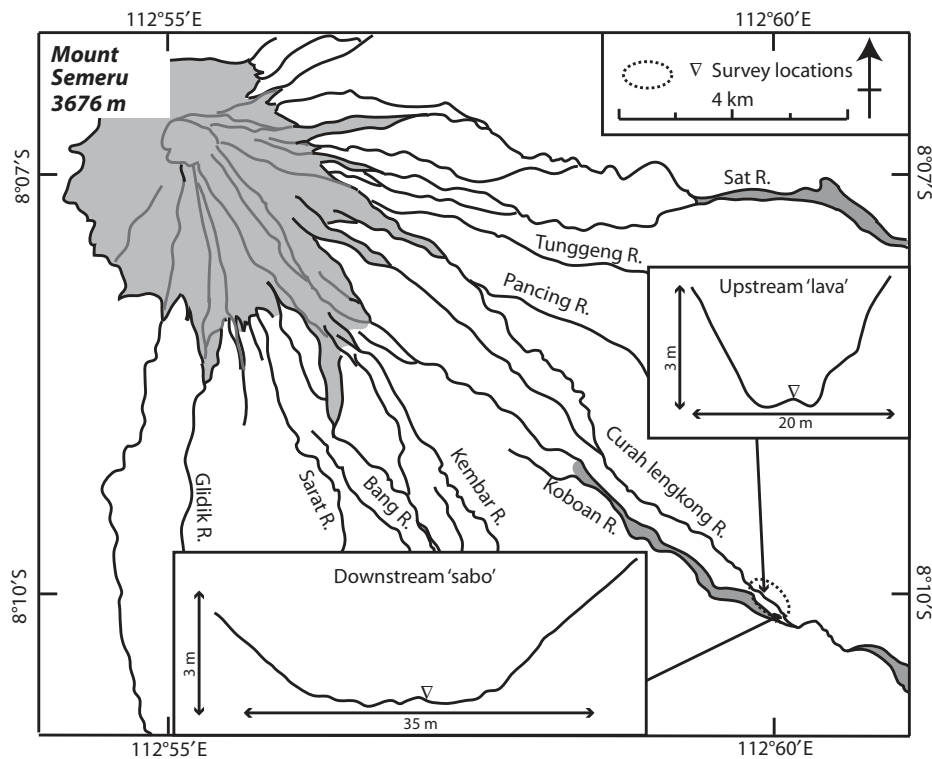


Figure 1. Location sketch map illustrating upstream “lava” and the downstream “sabo” sites, with an average slope of 3° between, after Doyle et al. (2010).

and evolution of the flow can be characterized. In this paper, we concentrate on flow velocity and volume calculations and demonstrate that flows can change considerably downstream, bulking by more than 100% between the two sites. These results enable a quantification of the bulking and debulking processes of lahars and definition of the conditions under which these contrasting behaviors may occur. The dominant behavior is shown to be controlled by the discharge and thus energy of the flow, a result applicable to solving entrainment-related problems encountered in other high-energy, solid-liquid, mass-flow systems, such as nonvolcanic debris flows, flash floods, turbidity currents, and industrial slurry transport processes. Such data are vital for the development of numerical descriptions of two-phase mass flows, especially those that can be applied to hazard mitigation and assessment tools.

We next discuss the definition of lahars, the current understanding of erosion and bulking processes, the field location and instrumentation, and the general characteristics of the flows recorded at Semeru. This is followed by a description of the methods used to calculate the velocities and volumes of the flow. The observed seismicity, velocity and wetted area at each site are then presented, followed by observations of

bulking and debulking, and a discussion of the controls on the dominance of each behavior, and the evolution of the flows downstream.

Lahars, Hyperconcentrated Flows, and Debris Flows

Lahars often begin as erosive watery floods or streamflow surges that entrain both sediment and water, developing a complex rheology, and transforming into hyperconcentrated flows and coarse and sediment-rich debris flows (e.g., Fisher and Schmincke, 1984; Costa, 1988). Hyperconcentrated flows are turbulent flowing mixtures of water and sediment that have a measurable yield strength, but are still able to flow as a liquid (Costa, 1988; Cronin et al., 2000; Pierson, 2005). They are intermediate in suspended sediment concentration between normal sediment-laden streamflow and debris flow. There are many criteria to determine hyperconcentrated flows (Pierson, 2005), and they have commonly been defined as having particle volume concentrations between 20% and 60% of clay, silt, and sand (Beverage and Culbertson, 1964). However, these concentration thresholds depend upon the grain-size distribution, and thus these flows are most accurately defined by a consideration of multiple factors, including their

sediment-transport mechanisms, hydrodynamic characteristics, and flow behavior (see Pierson, 2005). Vertical stratification often occurs in these flows, and a coarse pebble- and boulder-bearing bedload region is believed to underlie a dilute, fine-grained region (Pierson and Scott, 1985; Pierson and Costa, 1987; Cronin et al., 2000; Manville and White, 2003). Flow motion is driven by the fluid phase, with particles supported by buoyancy, turbulence, and dispersive grain forces (Smith, 1986).

Debris flows have much higher particle-volume concentrations, commonly above 60% (Pierson and Scott, 1985). However, this definition is again limited by the fact that particle-size distribution can strongly modify the flow properties (Pierson and Costa, 1987; Iverson, 1997). These largely unstratified viscoplastic flows have a high-yield stress (Coussot and Meunier, 1996; Coussot, 2005), where the particles are supported by the matrix strength and dispersive pressure between the grains (Smith, 1986). The flow rheology is variously described as plug flow, viscous fluid flow, or modified granular flow (Pierson and Costa, 1987; Iverson, 1997; Coussot, 2005). Most debris flows are characterized by a coarse-grained head of high concentration that dilutes into a liquefied slurry body and a watery tail (Vallance, 2000; Iverson and Denlinger, 2001). They are able to transport very large boulders that often migrate to the steep flow front, as well as to the flow margins where they form clear levees (Costa, 1988; Takahashi, 2007).

The formation of lahars (either with hyperconcentrated flow or debris-flow properties) from erosive watery floods or streamflow surges, depends upon an ample supply of easily erodible, fine-grained sediment to “bulk up” the flow (Scott, 1988; Scott et al., 1995). This entrainment often results in hyperconcentrated flows with complex flow rheology and behavior, where central portions of the flow tend toward debris-flow characteristics (Cronin et al., 1999, 2000). However, the ability of these erosive flows to entrain sediment not only changes their characteristics, it also increases their volume and discharge by several times (e.g., Pierson et al., 1990; Cronin et al., 1997; Hung et al., 2005). In addition, their mobility is greatly increased (Scott et al., 2005).

Empirical observations of lahars utilize a wide range of instruments, including the use of wire, ultrasonic, and radar sensors to measure flow depth, load cells to measure basal forces, pore-pressure sensors, video recordings, and electromagnetic Doppler speedometers, and more recently the study of seismic and acoustic signals via geophones, seismometers, and microphones (see summary in Arattano and Marchi,

2008). Seismic signals induced by lahars arise from the frictional interaction of the flow with channel walls, turbulent splashing, wave breaking, and particle collisions (Marcial et al., 1996; Cole et al., 2009). The magnitude of these induced ground vibrations has been found to be correlated to the flow depth and grain size (Arattano and Moia, 1999), and the discharge of the flow (Suwa et al., 2000). In addition, physical changes in the flow, its rheology and grain-size distribution produce different frequency responses (e.g., Okuda et al., 1979; Lavigne et al., 2000; Huang et al., 2004; Cole et al., 2009). Seismometers thus provide useful non-intrusive tools to monitor flow evolution.

Erosion and Bulking in Lahars

Evidence of bulking includes the presence of rock types in deposits that are not from the source location of the lahar (see review in Scott et al., 2005). During the September 1995 eruptions of Ruapehu, New Zealand, lahar deposits were commonly composed of only 5% juvenile material. The remainder of the flow material had been entrained along the flow path (Cronin et al., 2000). The amount of bulking of a lahar, commonly defined by the “bulking factor” (B.F.), has previously been calculated using a variety of methods (see summary in Fagents and Baloga, 2006). These include the ratio of the total volume of the flow or deposit to its initial volume (e.g., Scott et al., 2005; Fagents and Baloga, 2006), the ratio of the peak discharge at a location to the peak discharge at the source (e.g., Manville, 2004), or changes in the composition and lithology of deposits downstream, due to incorporation of external clasts, presence of juvenile material, or rounding of clasts (e.g., Thouret et al. 1998; Capra et al., 2002; Scott et al., 2005). The latter method depends upon the presence of sediments of different lithologies along the flow path. Estimates that consider only peak discharge may be misleading because discharge can also change due to shortening of the flowing mass and local velocity changes.

The degree of erosion-related bulking depends upon the erodibility of the channel bed, bank, and related material, the shear stress applied to these surfaces, and the volume of sediment available for erosion (Pierson, 1995). If basal erosion is limited due to a hard bedrock base, for example, then one can expect that lateral erosion and bank undercutting may dominate volume changes. Additional volume changes can occur by dilution due to tributary streamflows, over-running active stream channels, and entrainment of pore water (Pierson and Scott, 1985; Costa, 1988; Cronin et al., 1999). Light detection and ranging (LiDAR) data acquired before and after

the 2007 crater-lake outbreak lahar of Ruapehu volcano, New Zealand, indicate that the flow bulked by a factor of at least 3 within the first 5 km, after which alternating periods of net erosion and deposition occurred, being primarily controlled by changes in slope, channel confinement, and sediment availability (Procter et al., 2010). Similar observations have been observed from depositional evidence of a catastrophic precipitation-triggered lahar at Casita volcano, Nicaragua, by Scott et al. (2005).

Historical research into normal stream flow identifies that particle movement from the static bed occurs only when the destabilizing forces (drag, lift, and buoyancy) are greater than the stabilizing force of the particle’s weight (see summaries in Komar, 1988; Knighton, 1998). Once in the bedload region, turbulent mixing can cause the particles to migrate into suspension, depending upon grain size, shape, and density. Hence, for erosion to occur, the boundary shear stress must exceed a critical value, often defined by the Shields parameter. The average shear stress for turbulent river flow incorporates a molecular and an apparent eddy viscosity, both a function of the vertical velocity gradient. The eddy viscosity arises due to friction between adjacent eddies of water with different momentum (Knighton, 1998). As the sediment concentration of the flow increases due to entrainment, the fall velocity of particles decreases allowing fine sediment to remain in suspension for longer and, as the concentration approaches that of debris flows, the turbulence becomes damped (see summaries in Costa, 1988; Caruso and Pareschi, 1993). Laminar flow thus experiences a smaller shear stress and lower erosive capability for the same velocity gradient, as the eddy viscosity plays a lesser role (Leopold et al., 1995; Knighton, 1998). In addition, as the turbulence of the flow decreases, deposition via suspension related fallout is more likely to occur (Pierson, 2005). This is balanced by an increase in yield strength and particle-particle interactions that both act to keep material within the flow. In these high-concentration debris flows, deposition occurs via a combination of traction and vertical accretion, with en masse freezing occurring at the flow margins where the shear stress decreases (Major, 1997).

Lahar Recordings at Semeru

Figure 1 illustrates the survey location on the Lengkong river channel, 11.5 km from the summit of Mount Semeru, Eastern Java (Lavigne and Thouret, 2002; Lavigne et al., 2003; Lavigne and Suwa, 2004). Here the channel is composed of a ~30-m-wide box valley with a lava bedrock base overlain by thick gravels

with isolated bare patches. The banks are composed of loose lahar and pyroclastic deposits. In February–March 2008, we established two observation sites 510 m apart, the profiles of which are illustrated in Figure 1. The upstream “lava” site is characterized by a U-shaped channel with a bottom width of ~10 m, widening to 25 m at 3 m height. The downstream “sabo” site has a base width of ~20 m, broadening to ~35 m at 2.5 m height. These sites are ideal for observations, due to the relatively straight channel between them, the ease of accessibility, and the regular occurrence of rainfall-induced lahars during the rainy season. Instrumentation at both sites included (Doyle et al., 2009, 2010):

(1) Pore-pressure sensors installed mid-channel (Hobo U20 Water Level Logger and Solinst Levellogger Gold), and recording at 10 samples per second (sps) at the upstream site and 2 sps downstream. These sensors measure the pressure of the fluid between particles within the flow. If the sediment volume concentration remains below the maximum packing ratio of particles (~70 vol%), and circulation of the fluid within the lahar is aided by turbulence, then the fluid pressures are equalized throughout the flow, and the sensors can be used to infer a stage. These lahars are neither muddy nor cohesive, and thus we assume pure water in the pore spaces between particles. Thus, after correction for atmospheric pressure readings, a standard clear-water value of 1 kPa = 0.1022 m of water is used to convert from the pore-pressure readings to the fluid water height. This approach has been verified during the Ruapehu 2007 crater-lake outbreak lahar, where the calculated stage was found to agree to within <5% of radar stage gauge measurements, at both dilute and dense concentrations, with differences arising due to radar scattering from surface waves and splashing.

(2) Fixed 25 frames per second (fps) video cameras installed on the true left bank (looking downstream) of both instrument sites. The video footage is used to measure the surface flow velocities via particle image velocimetry (PIV; see Methods for Estimating Velocities and Volumes, and Dalziel, 2005). In addition, it is used to verify arrival times, as well as to make qualitative estimates of stage height, flow rheology, turbulence, and particle concentrations when direct samples were not possible (see below).

(3) A three-component Guralp CMG-6TD broadband seismometer was installed 10 m downstream of the upstream “lava” site, on the true left bank, with the North axis aligned parallel to the river bank. This recorded ground vibrations up to the Nyquist frequency of 62.5 Hz. Seismic amplitudes, frequency response, and signal directionality were calculated from the recorded seismic signal and were used to

estimate variations in sediment concentration, and to differentiate between the extremes of laminar and turbulent flow. In addition, the time of the signal associated with the lahar or wave front can be used to estimate body velocities, when compared to other available arrival time data at the downstream site.

(4) In the manner of Lavigne and Suwa (2004), direct suspended load sampling was conducted at the downstream site by dipping a 10 L bucket into the flow at 10–15 min intervals, when it was safe to do so. This provided samples to estimate the particle concentration, grain-size distribution, and rheological properties. Rheometric tests on this collected material are discussed further in Dumaisnil et al. (2010).

General Characteristics of Recorded Flows to Date

A total of eight rain-induced lahars were recorded during the field campaign of February–March 2008, with durations of 1–3 h (see Doyle et al., 2009, 2010; Dumaisnil et al., 2010, for summaries of initial findings). The available data collected during each event are listed in Table 1. When sampled concentrations were not available, qualitative descriptions of dilute, medium, or high concentration flows are interpreted from the video footage. This is calibrated against flow characteristics observed for those events with a full concentration data set. Sampled particle volume concentrations averaged between 28% and 44%. However, these concentrations are highly variable with minima of 15%–20% and maxima of ~70% (Table 1). Average grain-size distributions indicate 0%–12.9% gravel, 71.5%–90% sand, and 10%–16% silt and clay (Dumaisnil et al., 2010). Average concentrations are calculated within this grain-size distribution and, following Lavigne and Suwa (2004), do not include cobbles because the maximum analyzed grain diameter, determined by the sieve size, was 9 cm (Dumaisnil et al., 2010).

Flows commonly occurred very rapidly (<10–15 min) after the onset of heavy rainfall, with depths averaging 0.5–2 m, peak travel velocities of 3–6 m/s, and maximum discharges of 25–250 m³/s. These variable discharges can be compared to discharges of 50–500 m³/s calculated from video footage recorded at the downstream “sabo” site over the past six years (see Lavigne et al., 2003; Lavigne and Suwa, 2004). Visual and video observations indicate that all recorded flows were in the hyperconcentrated flow range, displaying various degrees of turbulence. At the highest sampled concentrations (>60 vol%), we characterize them as dense hyperconcentrated flows, because they show dampened turbulence (Doyle et al. 2009, 2010; and Seismicity, Veloc-

TABLE 1. A SUMMARY OF THE DATA AVAILABLE FROM OBSERVATIONS IN FEBRUARY–MARCH 2008 AT SEMERU VOLCANO, EAST JAVA

Event	Site	Peak stage (m)	Travel velocity, u_T (m/s)	Particle concentration (vol%)	Video footage available?
26/02/2008	Lava	0.5	N.A.	N.A.	60% [†]
	Sabo	0.2	1.1–1.7	10–23	Yes
28/02/2008	Lava	0.6	N.A.	N.A.	Yes
	Sabo	0.4	1.2–2.3	6–29	Yes
01/03/2008	Lava	2.0	N.A.	N.A.	No
	Sabo	1.6	2.9–7.5	18–67	Yes
04/03/2008	Lava	1.0	N.A.	N.A.	Yes
	Sabo	0.7	1.8–2.6	N.D.	Yes
05/03/2008	Lava	0.9	N.A.	N.A.	Yes
	Sabo	0.7	1.5–4.0	26–60	Yes
07/03/2008	Lava	1.0	N.A.	N.A.	55% [†]
	Sabo	1.0	1.8–3.6	9–23*	Yes
08/03/2008	Lava	1.4	N.A.	N.A.	No
	Sabo	1.0	2.0–3.7	N.D.	No
12/03/2008	Lava	1.3	N.A.	N.A.	Yes
	Sabo	1.0	2.1–4.6	N.D.	Yes

Note: The peak stage is calculated from the pore-pressure sensors, and the range of travel velocities is calculated from the distinct arrivals observed throughout the flow and identifiable at both sites (see General Characteristics of Recorded Flows to Date). The maximum and minimum sediment concentrations were calculated from bucket samples. The availability of video footage at both sites is also listed, and we note that seismic data are available for all events at the upstream “lava” site. Abbreviations: Lava—upstream site; Sabo—downstream site; N.D.—no data available; N.A.—not applicable.

*Bucket samples only taken during the last 30% of the lahar

[†]Video footage is not available for the full event; % available is shown.

ity, and Wetted Area, below). They were not fully evolved debris flows since they did not flow as a rigid plug, and bucket samples indicate that the flow was not able to suspend pebbles. This classification is further supported by sorting and grain-size analysis of body flow components by Dumaisnil et al. (2010).

Estimates of local Froude numbers indicate that all observed lahars were rapidly varied, unsteady, subcritical-turbulent flows for most of their duration, tending to critical and supercritical flow characteristics only at the discharge peaks, and subcritical-laminar flow during the highest concentration phases (see Doyle et al., 2010). Discrete, high-amplitude, onset arrivals were identified throughout each flow by rapid and emergent rises in stage, sharp increases in the seismic signal and its energy, and from video and visual observations (see example in Fig. 2). These distinct arrivals were not equivalent to the smaller superimposed waves often observed on debris flows (see: Iverson, 1997; Arattano and Moia, 1999; Massimo, 2000). This latter phenomenon is often attributed to “roll waves,” common in fluid flow down steep slopes (see: Takahashi, 2007; Zanuttigh and Lamberti, 2007). These roll waves usually have periods ≤ 100 s and are thus distinct from the 400–2000 s discrete gravity-flow phenomena we observed at Semeru. In addition, the observed subcritical flow conditions were not favorable for the formation of roll waves.

Debris-flow surges are described as having an abrupt bore at their head, with a high concentration of sediment and debris, followed by a gradually tapering, thin watery tail (Iverson,

1997, 2005; Vallance, 2000). The long discrete surges or pulses we observe in the Semeru lahars (Fig. 2) may be due to many spatially and temporally distributed lahar sources; ponding, damming, or surging of the flow (e.g., Arattano and Moia, 1999; Marchi et al., 2002; Zanuttigh and Lamberti, 2007); or the secondary entrainment of bed material, or fresh deposits, via the dilute tail sections of initial surges (Takahashi, 2007). These secondary discrete surges commonly travel slower than the flow front (see: Arattano and Moia, 1999; Hürlimann et al., 2003). However, the distinct arrivals traced between our sites at Semeru (Fig. 2) show different degrees of coalescence. In particular, those with the highest concentrations and wetted area traveled the fastest, catching up with the lahar front (Doyle et al., 2009, 2010).

The distinct multip peaked arrival phenomena recorded at Semeru occurred in hyperconcentrated flows, and are thus more dilute than the standard debris-flow surge. We herein refer to them as “packets” because their origins are as yet undetermined (Doyle et al., 2009); however, we believe they likely arise from dynamically independent lahars, originating from different tributaries or water sources along the middle and upper reaches of the Lengkong valley during a single meteorological event, or due to changes in rainfall intensity and location (Doyle et al., 2010). Detailed analysis of one example event, recorded on 5 March 2008, is discussed in Doyle et al. (2010). In this paper, we expand upon this work to include further analysis and interpretation of the surface velocity and volumes of all available events at both sites.

METHODS FOR ESTIMATING VELOCITIES AND VOLUMES

The footage recorded by the tripod-mounted video cameras provides continuous information about the surface of the lahars. We herein define the “surface velocity,” u_{surf} , as the instantaneous velocity calculated from this video footage, the “body velocity,” u_b , as the depth averaged velocity in the same location, assuming an average velocity profile (discussed further below), and the “travel velocity,” u_T , as the arrival velocity at the downstream “sabo” site, based upon the difference in travel time between the two sites. From the video footage, measurements of the surface-flow velocity have been collected using particle image velocimetry (Creutin et al., 2003; Dalziel, 2005). Velocity vectors were calculated from adjacent frames at intervals of 30 s. Considering an $\sim 4 \text{ m} \times 2 \text{ m}$ area on the flow surface, central to the channel, the average velocity vector was calculated. Outliers beyond one standard deviation of the average flow direction were omitted. These occur due to random flow motion, oversaturation of the image, and back scattering of light.

The average body velocity of the flow u_b is assumed proportional to the calculated surface velocity u_{surf} , via $u_b = ku_{surf}$. The value of the correction factor k is described by the vertical velocity distribution curve, which is commonly defined as being dependent upon the flow rheology, bed roughness, channel aspect ratio, particle volume concentration, and turbulence (Creutin et al., 2003). In an open channel, the velocity decreases logarithmically toward the bed. This can be described by the Prandtl-von Kármán “law of the wall” equation (Chow, 1959), from which a value of $k = 0.8$ is found for turbulent flow through a fairly rough channel (Matthes, 1956; Leopold et al., 1995). This increases to 0.9 as the channel resistance decreases (Klein et al., 1993). In general, for turbulent river flows and lahars, correction factors are assumed to be between 0.7 and 0.9 (e.g., Cronin et al., 1999; Hayes et al., 2002). However, a higher concentration of sediment leads to more laminar-type flow, as turbulent eddies are damped. For pure 1D laminar flow, $k = 0.5$ is more appropriate (Buchanan and Somers, 1969). It is unlikely that lahars ever reach fully laminar flow. The flows recorded at Semeru range from dilute to dense hyperconcentrated flow, and never reach full debris-flow behavior. Thus, to calculate the volumes, we assume an average behavior that is not fully turbulent. This is described by the pure-water correction factor of $k = 0.75$, and we quote the range of velocity and volume results for $k = 0.65$ and 0.85 to capture the range of velocities that may occur for more laminar or more turbulent flow.

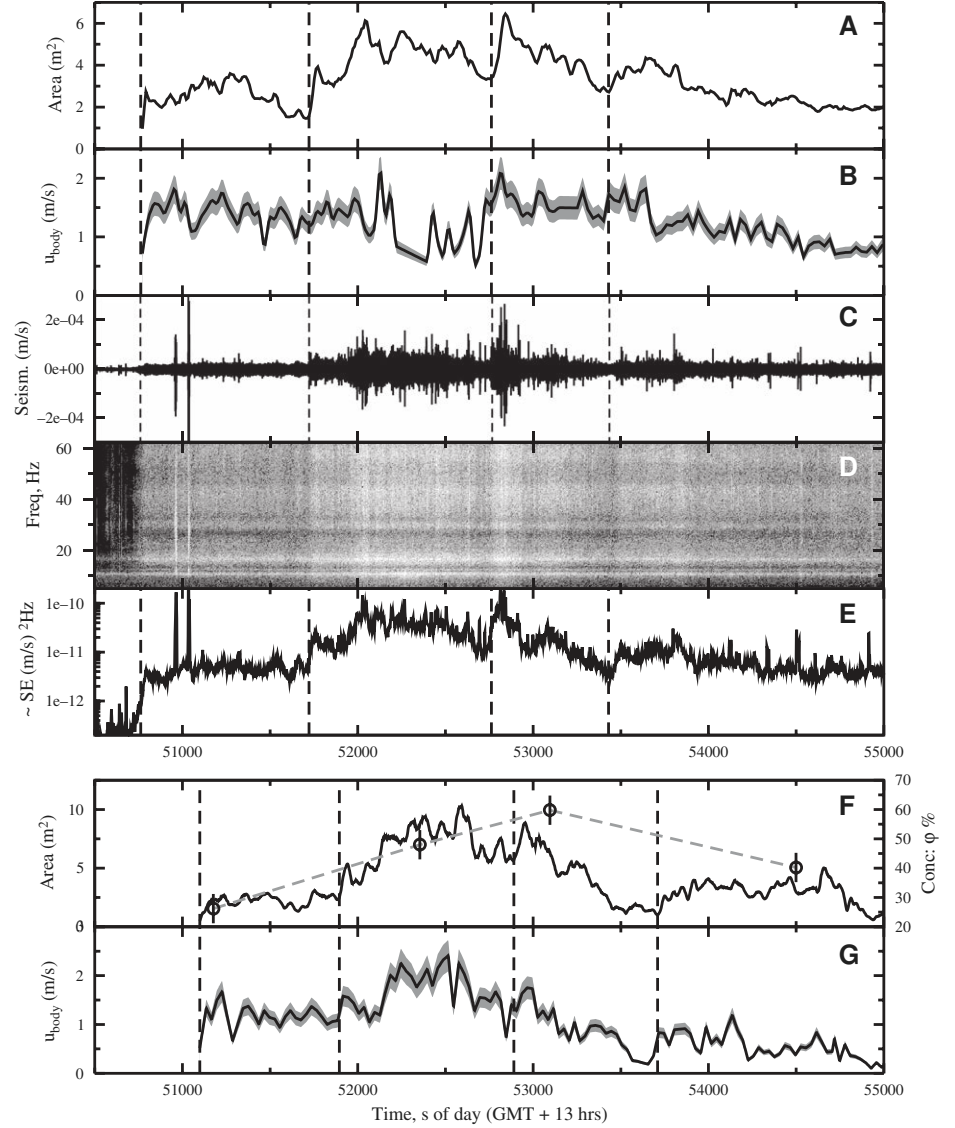


Figure 2. Lahar recorded on 5 March 2008. (A) The flow cross-sectional (wetted) area at the upstream “lava” site; (B) the associated body velocity as inferred from the surface velocity via $u_b = ku_{surf}$, assuming $k = 0.75$. Gray regions show the result if $k = 0.65$ or 0.85 is assumed instead; (C) the seismic ground velocity >5 Hz perpendicular to the channel; (D) the associated spectrogram showing the seismic frequency distribution, calculated using a migrating 1024 sample point window with a 50% overlap; (E) the approximate energy in this seismic signal; (F) the wetted area at the downstream “sabo” site and the sampled concentration (circles); and (G) the associated body velocity at the downstream “sabo” site as calculated in (B). Vertical dashed lines indicate packet arrivals. Adapted from Doyle et al. (2010). At the downstream “sabo” site, packet 3 has a sampled particle concentration of ~ 60 vol% and travels at $\sim 4.0 \pm 0.3$ m/s between sites, whereas packets 1 and 2 have concentrations of ~ 26 vol% and ~ 48 vol% and travel at $\sim 1.5 \pm 0.1$ m/s and $\sim 2.9 \pm 0.2$ m/s, respectively.

To calculate the discharge and cumulative volume of each lahar, the 30 s interval body velocity data are interpolated to the pore-pressure sampling times. In addition, the pore-pressure stage records are converted to flow cross-

sectional area (wetted area) records using global positioning system (GPS) profiles of each site, and smoothed with a 20 s averaging window. From simple geometry, the total “length,” L , of the lahar from its flow front is calculated via:

$$L = \sum_{i=i_{arr}}^N \left(\frac{(u_b^i + u_b^{i+1}) \Delta t}{2} \right), \quad (1)$$

for a total of N recordings over time, t , where i represents the individual measurements recorded at intervals of $\Delta t = t^{i+1} - t^i$. This total “length,” L , is calculated from the onset of the rising limb of the stage record ($i = i_{arr}$). From this, the total volume, Vol , of the passing lahar is thus:

$$Vol = \sum_{i=i_{arr}}^N \left(\frac{A^i + A^{i+1}}{2} (L^{i+1} - L^i) \right), \quad (2)$$

where A is the wetted area of the flow. The average discharge of the flow, Q , between two time recordings is:

$$Q(t^{i+1}, t^i) = \frac{1}{2} (A^i u_b^i + A^{i+1} u_b^{i+1}). \quad (3)$$

This method is similar to that discussed by Aratano and Marchi (2008). However, their calculations utilize a mean velocity over the duration of the flow, where the mean front velocity is often used as a surrogate. They do not include the significant variations in instantaneous flow velocity, and hence discharge variations, that can occur during the passage of the lahar.

SEISMICITY, VELOCITY, AND WETTED AREA

Figures 2, 3, and 4 display examples of three recorded flows on 4, 5, and 12 March 2008, illustrating the cross-sectional area interpreted from the pore-pressure stage records (A), the body velocity interpreted from the video footage (B), the seismic data (C–E) at the upstream “lava” site, and the associated available data at the downstream “sabo” site (F and G). Individual “packets” (see General Characteristics of Recorded Flows to Date) within these lahars can clearly be identified by changes in stage, wetted area, sharp increases in the seismic signal, and changes in the seismic frequency distribution. These changes are supported by video and human on-site visual observations, where the lahar onsets are commonly recognized by an emergent and rapidly rising stage, not a steep moving front. For many of the sampled events, the highest sediment concentration lags this onset (e.g., Fig. 2F).

Changes in particle concentration and grain-size distribution are expected to produce different frequency responses in the generated seismic signal (Marcial et al., 1996; Lavigne et al., 2000; Huang et al., 2004; Cole et al., 2009). Sliding frictional bedloads produce lower frequency signals than particle collisions

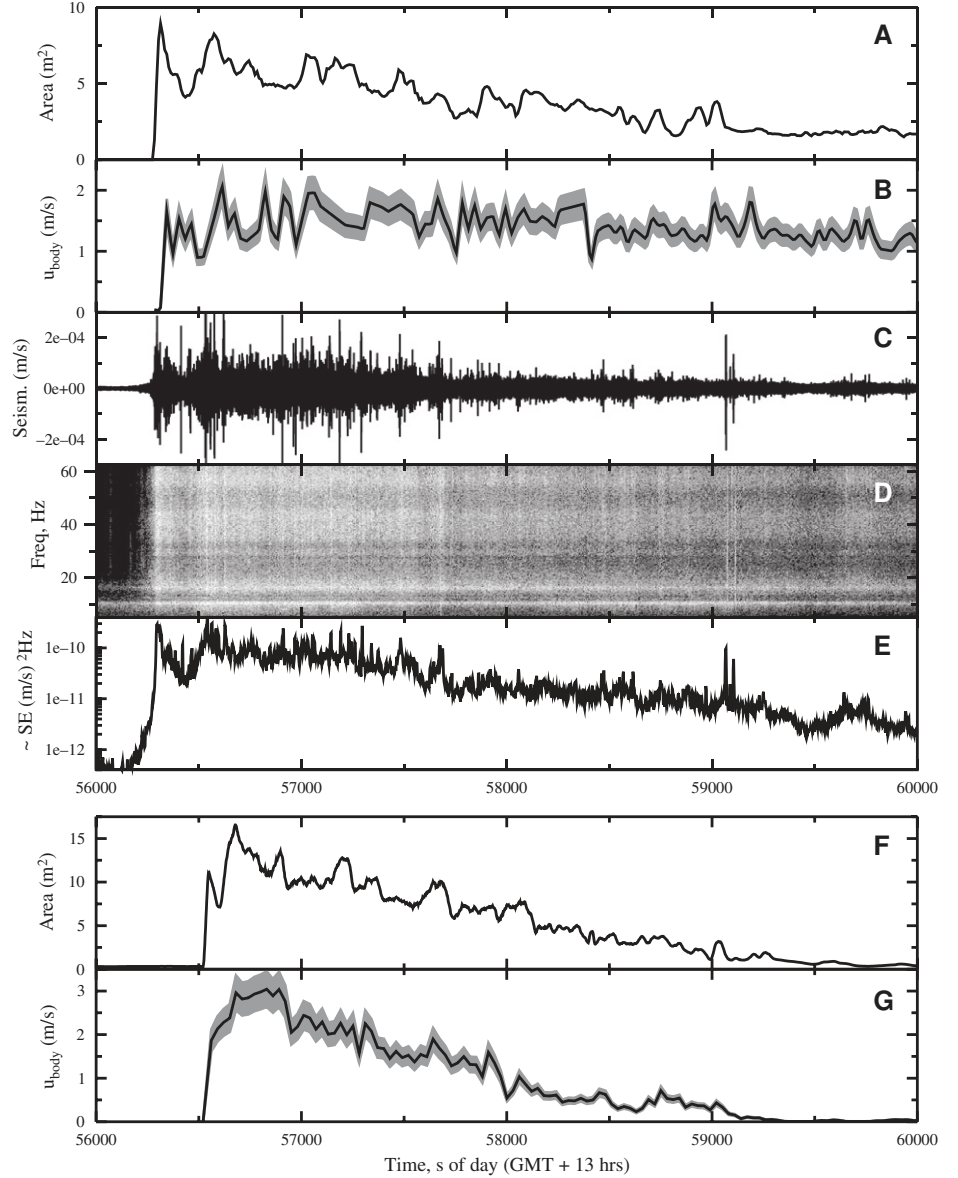


Figure 3. Lahar recorded on 12 March 2008. Details same as given for Figure 2.

(Huang et al., 2004). Hence, laminar sliding flows, such as snow slurry lahars, are dominated by lower frequencies (5–20 Hz), while turbulent hyperconcentrated flows have dominant vibrations above 30 Hz (Cole et al., 2009). Previous analysis of the event of 5 March 2008 (Doyle et al., 2009) identified that the recorded flow induced a broad frequency response. This is now identified for all recorded flows (e.g., Figs. 3D and 4D). The spectrograms illustrate that, while the frequency response increases in intensity as the stage, area, and concentration of the flow increases, the seismic frequency distribution does not change. This suggests that the flows were broadly turbulent throughout, with both frictional and collisional processes still occur-

ring at high concentrations. Visual observations support this hypothesis, with some minor wave breaking at the highest concentrations.

For the very highest recorded concentrations, there is a slight decrease in the seismic energy than what would be expected for the corresponding wetted area (e.g., 1 March 2008 and packet 3 of 5 March 2008, Fig. 2). As solid content increases, turbulence is expected to reduce (Costa, 1988; Caruso and Pareschi, 1993). This suggests that while turbulent particle collisions may still occur (broad frequency response), the high concentration of particles may actually dampen some of this turbulence, producing seismically quieter flow. Video footage indicates that the number of waves breaking on

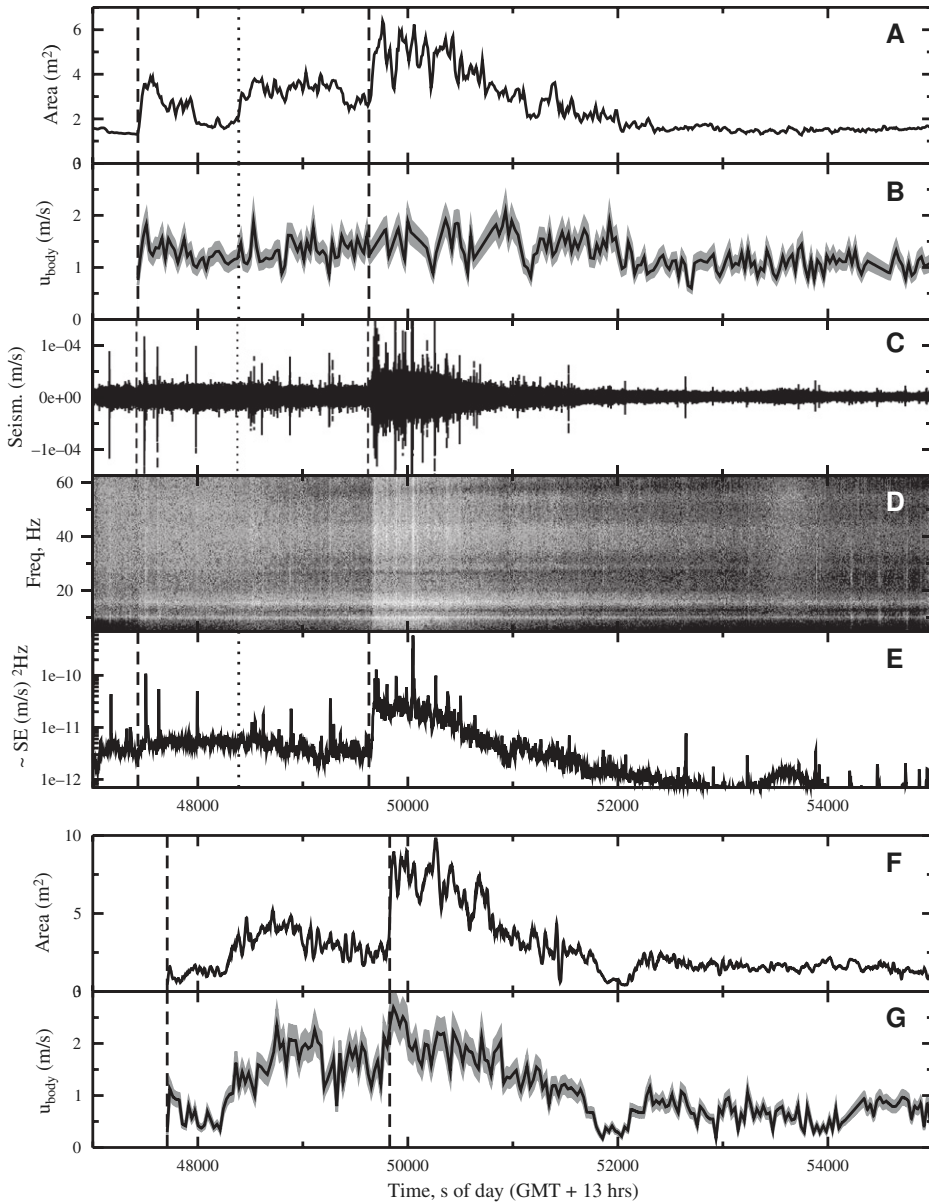


Figure 4. Lahar recorded on 4 March 2008. Details same as given for Figure 2.

the flow surface decreases during these high-concentration periods of flow, and the flowing mixture develops a thick, oily consistency suggestive of a more laminar-type flow. At these high concentrations, the flows can be described as transitional hyperconcentrated flows, which have started to acquire debris-flow characteristics. However, they were not full debris flows, they do not behave or travel as rigid plugs, and bucket sampling illustrates that the flows are not yet able to support pebbles and dense sediment (Dumaisnil et al., 2010)

Except for the regions with the highest volumetric particle concentrations (>60 vol%), the logarithm of the seismic energy (SE) correlates

extremely well with the wetted area (e.g., Figs. 2A and 2E versus 3A and 3E), where the quieter flows represent the less turbulent, dense hyperconcentrated flows. Unsteady surging flow and packet onsets can be identified, in the logarithm of the seismic energy, which does not appear to be affected by any changes in body velocity. These data indicate that for all recorded flows with particle concentrations $\phi < 60$ vol%, $\log SE$ is a good proxy for the flow cross-sectional (wetted) area (Figs. 2–4). This is in agreement with Tuñgol and Regalado (1996), Suwa et al. (2000), Massimo (2000), and Huang et al. (2004), who correlate the peak seismic signal with the peak discharge. Arattano and Moia

(1999) suggest that grain size may also be important, producing different signal intensities and seismic frequency distributions. This may be an additional explanation for the lower seismic energy observed at the highest particle concentrations.

Body Velocity

The body velocity, u_b , correlates well with the peak wetted area, particularly at the downstream “sabo” site (e.g., Figs. 2F, 2G, and 3), due to the larger wetted areas commonly observed at this site. For those events where the wetted area is larger at the upstream “lava” site, the correlation there is improved (e.g., 28 February 2008).

Previous analysis (Doyle et al., 2009, 2010) identified that the packets with the highest concentration and wetted area are traveling the fastest, catching up with the flow front. This effectively shortens the total length of the lahar as the individual packets coalesce (see General Characteristics of Recorded Flows to Date). For the event of 5 March 2008, the peak body velocity at the downstream “sabo” site occurs during packet 2, with a value of $u_b = 2.4 \pm 0.4$ m/s. However, packet 3, which has the highest sampled concentration (60 vol%), has a travel velocity between sites of $u_r \approx 4.0 \pm 0.3$ m/s, while packet 2 travels at $u_r \approx 2.9 \pm 0.2$ m/s. This difference between peak travel and local body velocities may arise from an incorrect velocity distribution curve used in the body velocity calculations (see Methods for Estimating Velocities and Volumes). If an end member, fully turbulent correction factor of $k = 0.9$ is assumed, then the maximum likely peak body velocity for this lahar would be $u_b = 2.9 \pm 0.4$ m/s.

The differences between the travel and local body velocities are not apparent for all recorded events. For the 4 March 2008 lahar, the downstream localized peak body velocity of $u_b = 2.7 \pm 0.4$ m/s (for $k = 0.75$) occurs at the onset of the second packet, and agrees with a travel velocity of $u_r = 2.6 \pm 0.1$ m/s (Fig. 4). For the 12 March 2008 event, the downstream peak body velocity of $u_b = 3.0 \pm 0.4$ m/s corresponds to the peak of flow, which travels at $u_r = 3.4 \pm 0.2$ m/s (Fig. 3). Arattano and Grattoni (2000) found that localized surface velocities interpreted from video footage were $\sim 10\%$ less than travel velocities between two sensors. They attribute this difference to localized acceleration or deceleration of the travel velocity along the flow path. Our travel velocities are averaged over a 500 m flow path, while the body velocities are averaged over an area of 8 m^2 for greatest PIV accuracy. These later velocities represent instantaneous local velocities, which may well vary along the

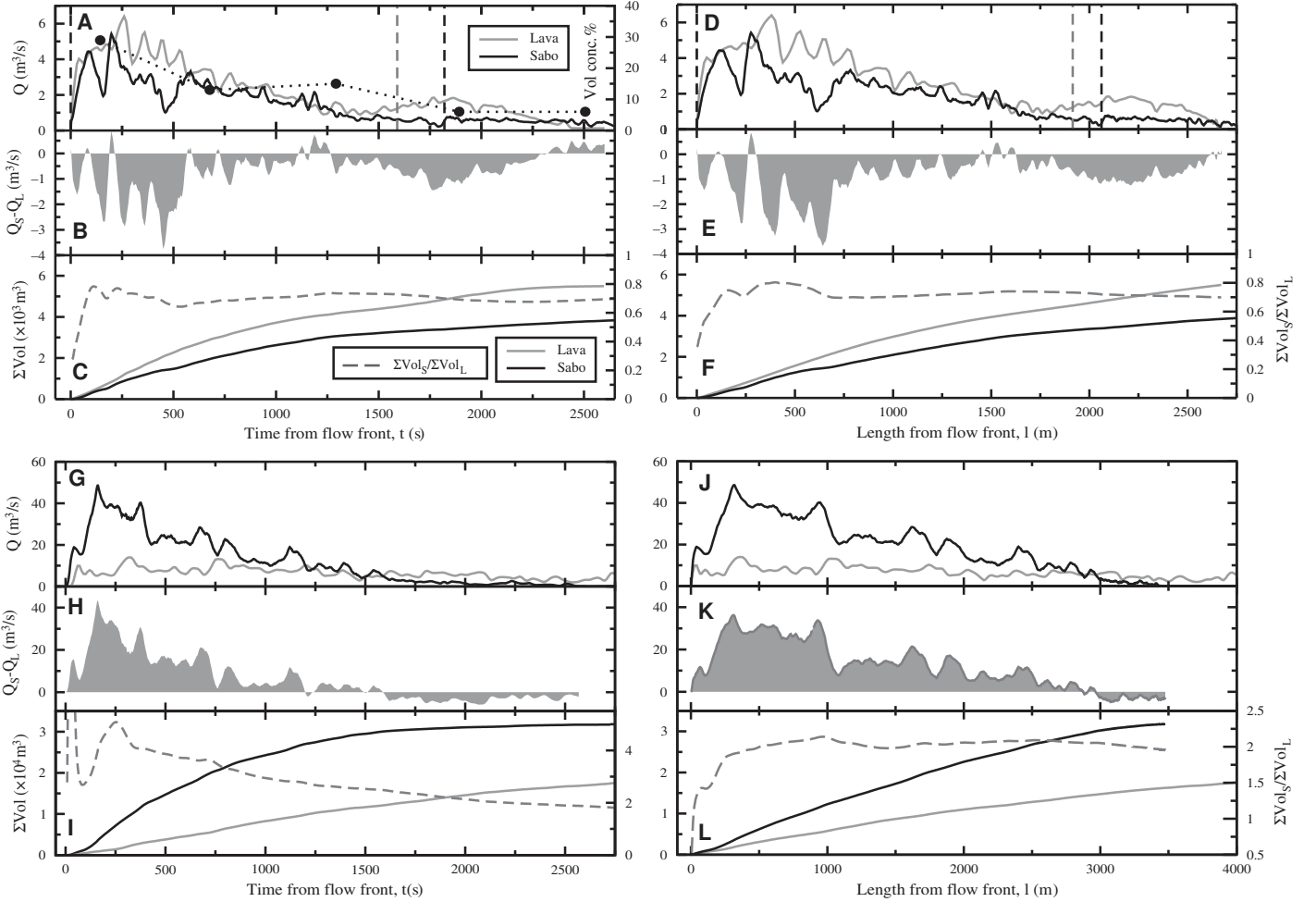


Figure 5. Examples of flows that exhibit either dominant debulking behavior (A–F) or dominant bulking behavior (G–L). (A) 28 February 2008: The discharge calculated at both sites, from the wetted area and the body velocity, $u_b = 0.75u_{surf}$, with respect to the time of the flow from the flow front; (B) the difference between the discharge at both sites, illustrating debulking; (C) the cumulative volume calculated at each site, and the ratio between them; (D–F) the same parameters plotted with respect to the length of the flow from the flow front. This length is calculated from u_b at each sample time; and (G–L) bulking behavior on 12 March 2008, same key.

500 m flow path. Additional differences may arise from local light or turbulence effects in the PIV capture method, and from subtle channel bends that may induce accelerations and decelerations of the flows between sites. We assume that the calculated body velocities are robust, allowing for discharge calculations and comparisons at both sites. Future analysis may consider a larger region for the PIV analysis, to average out some of these localized variations.

VOLUME CHANGES: BULKING AND DEBULKING

As portions of the lahar catch up with the flow front, they effectively shorten the length of the lahar. To accurately compare packets at both sites in a graphical manner, we have mitigated these “shortening effects” by depicting the

calculated discharges with respect to the length from the flow front, as well as the arrival time (Figs. 5A and 5D). This length is calculated from the body velocity and the recording times, allowing for a direct comparison of the wave between sites. For the event of 28 February 2008 (Figs. 5A–5F), there was a net decrease in discharge between sites. The peak discharge drops from $6.4 \pm 0.9 \text{ m}^3/\text{s}$ at the upstream “lava” site to $5.4 \pm 0.7 \text{ m}^3/\text{s}$ at the downstream “sabo” site (Figs. 5A and 5D), where the ranges correspond to $u_b = (0.75 \pm 0.10)u_{surf}$. However, to truly determine whether a volume change has occurred, we calculate a bulking factor of the lahar based on either the total volume within each individual packet, or the total volume of the entire lahar. This is calculated by integrating under the discharge:time curves. When these results are compared to the change in the length

of the lahar, or the individual packet, periods of bulking due to entrainment-related volume changes can be isolated from periods of bulking due to shortening, where the discharge may have changed with the length and velocity of the lahar. For each lahar that has video footage at both sites, these results are illustrated in Table 2. For the event on 28 February 2008 (Figs. 5A–5F), by the end of the first packet, the cumulative volume has decreased by a factor of 0.8 between sites, and the packet length has increased by a factor of only 1.08. This indicates that debulking has dominated this flow as it traveled downstream between the two sites.

For the event of 12 February 2008 (Figs. 5G–5L), we see contrasting behavior. There is a net increase in total discharge between sites, suggesting that the flow bulked. The peak discharge increases from 14 ± 2 to $49 \pm 6 \text{ m}^3/\text{s}$ (Figs. 5G

TABLE 2. THE VOLUME CALCULATED FOR EACH INDIVIDUAL PACKET AND FOR THE TOTAL LAHAR, RECORDED AT THE UPSTREAM “LAVA” SITE (ΣVOL_L) AND THE DOWNSTREAM “SABO” SITE (ΣVOL_S)

Event	Packet	ΣVol_L (m ³)	ΣVol_S (m ³)	$\Delta \Sigma Vol / \Delta x$ (m ³ /m)	Vol B.F.	L ratio	T ratio	Q_{ave} ratio	Q_{max} ratio
26/02/2007	p1	678	148	-1.0	0.22	0.77	1.00	0.22	0.24
	p2	4439	1087	-6.6	0.24	0.72	0.87	0.27	0.36
	Total*	5116	1235	-7.6	0.24	0.73	0.90	0.25	0.36
28/02/2007	p1	4496	3386	-2.2	0.75	1.08	1.14	0.67	0.85
	p2	1001	494	-1.0	0.49	0.90	1.00	0.49	0.42
	Total	5497	3880	-3.2	0.71	1.03	1.08	0.62	0.85
04/03/2007	p1	8315	8632	0.6	1.04	1.01	0.96	1.11	1.48
	p2	13,601	18,003	8.6	1.32	0.92	1.00	1.32	2.27
	Total	21,915	26,634	9.3	1.22	0.96	0.98	1.23	2.27
05/03/2007	p1	3362	2093	-2.5	0.62	0.70	0.84	0.75	0.78
	p2	5157	12,040	13.5	2.33	1.39	0.96	2.45	2.25
	p3	4565	3691	-1.7	0.81	0.69	1.22	0.66	1.26
	p4	6149	3097	-6.0	0.50	0.51	1.00	0.50	0.56
	Total	19,232	20,921	3.3	1.09	0.76	0.99	1.16	1.89
07/03/2007	p1	7696	9144	2.8	1.19	1.36	1.00	1.19	1.56
	p2	5514	11,888	12.5	2.16	1.41	0.87	2.49	2.46
	Total*	13,210	21,032	15.3	1.59	1.38	0.95	1.91	2.46
12/03/2007	Total	18,237	31,731	26.5	1.74	0.80	0.95	2.29	2.23

Note: The rate of bulking and debulking per meter of travel distance is also shown ($\Delta \Sigma Vol / \Delta x$). The volume bulking factor (Vol B.F.) and the ratio between sites of the length (L), time duration (T), average discharge (Q_{ave}), and peak discharge (Q_{max}) are also shown. The end of the event is identified from visual observations and, where possible, when the discharge returns to within 10% of the base level.

*Video data were not available for the full duration of all events, and so the total is calculated based only on the complete packets recorded.

and 5J), corresponding to a peak wetted area increase of 5 ± 1 to 9 ± 2 m². This increase in discharge and wetted area may be caused by a decrease in the lahar length downstream, and thus a shortening or compressing of the flow. However, as illustrated in Table 2, the total lahar has bulked by a factor of 1.8 between sites, while being shortened by a factor of only 0.8, indicating that erosion-related bulking is dominant. Most of this bulking occurred shortly behind the head of the wave (Figs. 5K and 5L), which corresponds to the region of high wetted area and seismic energy (Fig. 3).

Some flows exhibit periods of both bulking and debulking (e.g. Fig. 6). For these events, the onset of the wave was characterized by a debulking of material. The peak discharge, and peak bulking occurred in the main body of the wave, followed by debulking during the tail. For the event of 5 March 2008 (Figs. 6G–6L), the first packet decreases in total volume between sites by a factor of 0.6 (Table 2). This packet is very dilute (26 vol%) and thus most likely had a low rate of sediment deposition, due to the low concentration of particles in the flow. Alternatively, the decrease in discharge may have been due to water draining into the pore spaces of the substrate (c.f. Manville, 2004; Scott et al., 2005). Prior to the arrival of the lahars, the river bed can be considered almost dry. If an active water channel is present, it usually occupies a narrow (<1 m) region of the wide (30 m) channel, and outside this region the infiltration rates are quite high. If the onset of the flow is effectively saturating the basal material, then the substrate may become more susceptible to mobilization

and entrainment by the following portions of the lahar. This would further aid the bulking process, where the total volume of packet 2 increased by a factor as high as 2.3 (Table 2).

In the case above, it is also important to consider that the front of packet 2 is catching up with the flow front, and thus its length has increased by a factor of 1.4 by the time it reaches the downstream “sabo” site. In turn, the length of packet 1 has decreased by 0.7 (Table 2). It does not appear that packet 1 is being compressed by the accelerating packet 2, because its average wetted area decreased from 2.5 ± 0.6 to 2.2 ± 0.5 m² between sites (Fig. 2). However, if packet 2 actually consumed some of packet 1 ahead of it, this cannibalization would account for a factor of up to 1.4 of the bulking of packet 2. A remaining factor of up to 1.7 would be due to entrainment of the substrate, collapse of the channel walls, and inclusion of surface rain water. Rainfall intensity is of the order of 10–20 mm/hr, and is usually only sustained for a few tens of minutes. Thus, a direct rainfall input into the moving lahar between sites would be of the order of 100–300 m³ for the slowest lahars, making up only a small fraction of their volume changes, which were typically $\gg 1000$ m³ (Table 2). During the subsequent packets of the 5 March 2008 lahar, the flow wanes and debulking dominates, such that by the end of the lahar the total volume increased by only 10%. However, within the wave, packets bulked by factors as high as 2.3, corresponding to peak discharge increases of 89%. Similar behavior is observed for the events recorded on 4 and 7 March 2008 (Figs. 6A–6F and Table 2).

DISCUSSION

Controls on Bulking and Debulking Behavior

The progression from hyperconcentrated to debris-flow sediment concentrations has been observed in many small, rain-induced lahars (Marchi et al., 2002; Lavigne and Suwa, 2004). Our flow data demonstrate that bulking, debulking, and periods of both processes occur in these flows. The switch between behaviors may be due to the increase or decrease in erosive energy as the discharge of the flow changes, or changes in the process of erosion as flow depth variations promote a dominance of either channel bed removal, undercutting of banks, or direct bank erosion. Visual observations since 2002 at the Lengkong channel suggest that lateral erosion has gradually become more important as the lava bedrock base is exposed and bank undercutting occurs. However, during our field study in 2008 visual observations indicate that basal erosion and deposition were still dominant. Minor lateral erosion and bank undercutting occurred, making only a small contribution to the volume changes between sites.

Historical observations indicate that faster moving, or deeper, flows have a greater ability to entrain sediment through turbulence and tractive shear stresses (see summary in Fagents and Baloga, 2006). In addition, subcritical flow is characterized by greater deposition rates than supercritical flow (Pierson, 1995). The recorded Semeru events are rapidly varying, unsteady, subcritical-turbulent flows for most of their duration, tending to critical and supercritical conditions during their flow peaks (Doyle et al., 2010). Figure 7 illustrates the relationship between the volume change for each packet (A and B), or for the total event (C and D), and the average or the peak discharge at the upstream “lava” site. The smaller discharge events lose material between sites and the larger events, by contrast, gain material. The dominant behavior is thus controlled by a threshold, described by an average discharge value at the upstream site of $\sim 3.5 \pm 0.5$ m³/s, and a peak discharge of $\sim 7.5 \pm 1.0$ m³/s.

The lahar recorded on 5 March 2008 may be an exception to this. Its third packet does not appear to be controlled solely by a discharge threshold (Figs. 7A and 7B). It exhibited a debulking regime, even though its peak and average discharges suggest it should be bulking. As discussed in the previous sections, erosion and incorporation of sediment results in an increase in both particle concentration and bulking of the flow volume. Near the onset of packet 3, the concentration reached 60 vol%, and the lahar

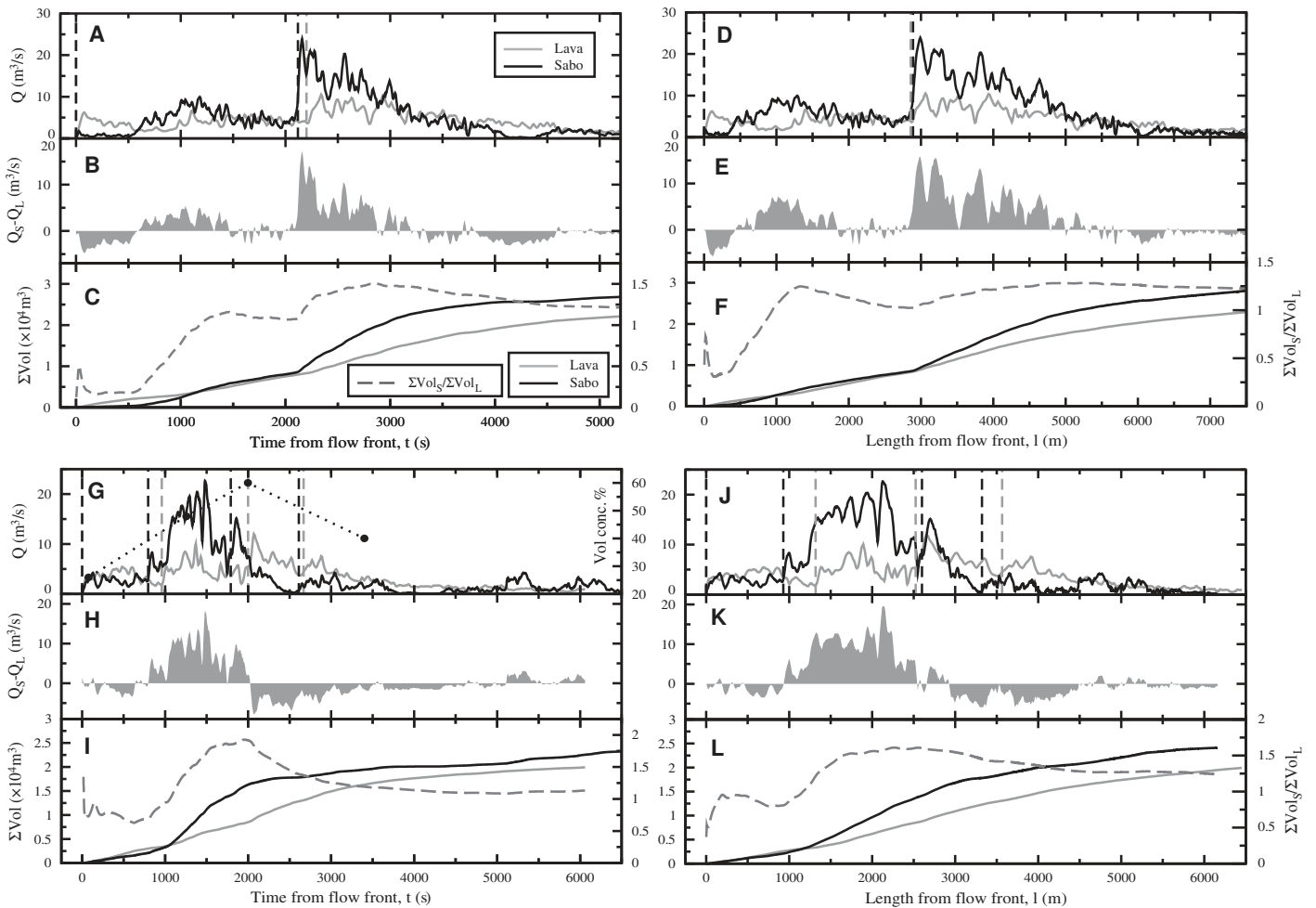


Figure 6. Examples of events that illustrate both bulking and debulking behavior at distinct times within the flow. Shown are the events of 4 March 2008 (A–F) and 5 March 2008 (G–L). Details same as given for Figure 5.

behaved like a dense hyperconcentrated flow, starting to acquire some debris-flow characteristics (Fig. 2). Shortly after this peak there was a change in erosive behavior, and a discharge decrease between sites (Figs. 6G–6L), even though the discharge was above $5 \text{ m}^3/\text{s}$ at the upstream “lava” site (Fig. 7). This suggests that the high particle concentration caused a premature switch in behavior. This high concentration may have dampened the turbulence of the flow, resulting in a lower erosive capability, and a greater propensity to deposit particles (see Introduction).

As discussed in Erosion and Bulking in Lahars, erosion requires the boundary shear stress of a flow to exceed a critical value, often defined by the Shields parameter (Knighton, 1998). The average shear stress incorporates a molecular and apparent eddy viscosity, which are both a function of the vertical velocity gradient. We propose a simplified pattern of erosion and deposition in these rain-induced lahars. When

the flow is turbulent and dilute, the presence of turbulent eddies makes a significant contribution to the average shear stress, and erosion of particles is possible if the discharge is high. Flow resistance could be described by Manning’s or Chezy’s laws (Chen, 1987; Macedonio and Pareschi, 1992), which both consider the effect of channel roughness on flow velocity. As these flows entrain material they increase in both concentration and discharge. If the particle concentration stays below 60 vol%, then turbulence will still play a role. The average basal shear may be best described by turbulent dilatant resistance terms (e.g. Takahashi, 1991; Macedonio and Pareschi, 1992), which depend upon the velocity of the flow. Hence, while the flow has a high discharge and travel velocity, the basal shear may still exceed the critical Shields’ parameter for erosion (see our Introduction, and the summary in Komar, 1988). The flow thus bulks between sites. However, when the flow starts to wane, its erosive energy

and sediment-carrying capability decreases, and it debulks between sites.

Alternatively, if the particle concentration exceeds 60 vol%, the turbulence in the flow may be dampened to such a degree by the presence of particles (see Seismicity, Velocity, and Wetted Area) that the eddy viscosity plays a lesser role in the basal shear stress for the same velocity gradient (see Lahar Recordings at Semeru), and the erosive capability will drop. However, this behavior is balanced by the increase in fluid density, which would increase the basal shear stress. Thus, at the threshold point where turbulence is considerably damped but concentration has not increased greatly, entrainment may decrease, and debulking may occur, even if the flow has a high discharge (e.g., 5 March 2008; Table 2 and Fig. 7). The decrease in sediment concentration may return the flow to an erosive regime, and the cycle may continue. In addition, the channel geometry and variation in the channel-bed gradient may trigger further

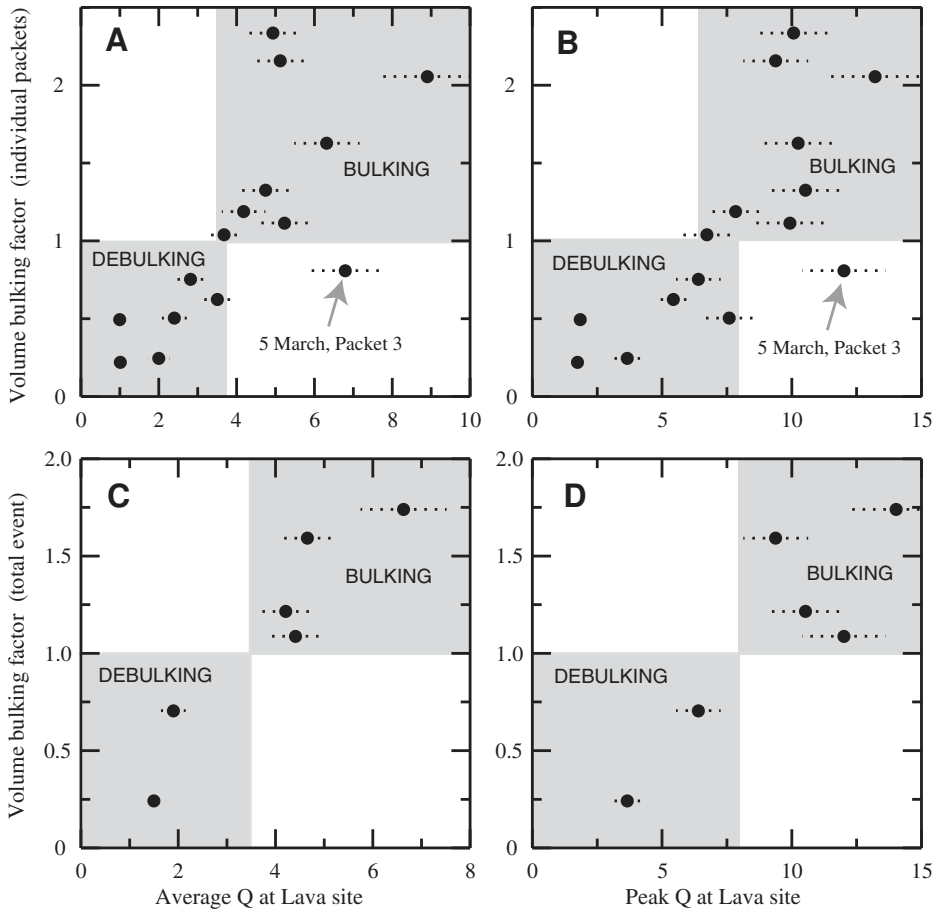


Figure 7. The relationship between bulking or debulking behavior and the average or peak discharge Q at the upstream “lava” site for individual identified packets (A and B) and total event (C and D) changes. All discharges shown assume a body velocity $u_b = 0.75u_{surf}$, and vertical bars indicate the range for factors of $k = 0.65$ and 0.85 .

changes to erosive or depositional behavior (c.f. Procter et al., 2010), due to an increase of undercutting or surface erosion of the channel banks, or changes in flow velocity and thus erosive capability.

Evolution of These Flows Downstream

The peak particle concentration commonly lags the front of these rainfall-induced lahars (e.g., Petts et al., 1985; Scott, 1988; Vignaux and Weir, 1990; Lavigne and Suwa, 2004). This can occur due to a celerity effect where the wave front travels faster than the wave material (Petts et al., 1985; Vignaux and Weir, 1990), due to the fluid component separating and propagating ahead of the sediment-rich component (Scott, 1988), or due to a high-concentration lahar pushing a wave of native water ahead of it (Cronin et al., 1999). However, for these Semeru lahars, neither of these processes actually occurs, because the packets with the

peak concentration, associated with the highest stage, were traveling faster between sites and were catching up with the flow front (see General Characteristics of Recorded Flows to Date, and Doyle et al., 2010). Lavigne and Suwa (2004) have observed that the peak concentration can occur in such hyperconcentrated flows at the front, mid-point, or back of the flow. Using numerical models of the transport of fine sediment by a flood surge, Pritchard (2005) identified that when a simple erosional model is adopted for a dilute well-mixed suspension, then the maximum concentration occurs at the flow front, because it has been erosional for longest and flows the fastest (see also Pritchard and Hogg, 2002, who model sediment transport under dam-break flow). This model assumes that the entrainment rate depends upon the power of the excess shear stress above a critical value (Dyer and Soulsby, 1988). If, however, the erosion is calculated in terms of a dimensionless frictional velocity based on

the Chezy drag law (Garcia and Parker, 1991), Pritchard (2005) finds that the peak concentration occurs within the body of the flow, thus the hindmost parts of the surge may transform into a sediment-laden, dense, hyperconcentrated flow before the front does.

For the recorded flows at Semeru, we assume that the peak concentration is located where the wave has been erosive for longest, which is often the largest packet located mid-lahar. We have also assumed that these lahars are composed of many discrete individual lahar packets, originating from multiple sources feeding into the main channel, and showing different degrees of coalescence at the instrument sites (see General Characteristics of Recorded Flows to Date and Doyle et al., 2010). Thus, the peak in concentration may actually correspond to the lahar packet that has either been in an erosional regime for longest, or had the longest travel path over which erosion can occur. In addition, if these later packets are traveling over a substrate that has been saturated by the head of the lahar, then further entrainment of particles may be facilitated (Scott et al., 2005). While these packets are still able to entrain sediment, and increase in concentration, they will continue to travel faster and continue to catch up with the flow front. The peak concentration will consequently migrate toward the flow front, and eventually it may develop a debris-flow-type behavior and structure. This could be a “debris-flow wave” structure, described by Marchi et al., (2002) to be a wave of sediment and water with a small, hyperconcentrated pre-surge, very shortly followed by a large, steep fronted, debris flow that then dilutes back to a hyperconcentrated flow. Thus, the ability for some packets to entrain at a greater rate than others may actually drive further coalescence of these individual lahar packets, forming one coherent lahar wave.

CONCLUSIONS

The bulking of lahars generate an extreme hazard to low-lying and distal areas. Empirical field observations offer an opportunity to quantify and constrain the processes driving both bulking and debulking, leading to a greater understanding of their controls. Our results indicate that the use of two, closely located instrument sites (510 m apart) provides a more accurate characterization and physical understanding of these complex flows, vital for the development of numerical descriptions used in hazard mitigation tools. Models that incorporate bulking, concentration, and volume changes (e.g., Fagents and Baloga, 2006) and river-supply sediment-transport models

that consider high suspension loads (e.g., Cao et al., 2006) are very promising avenues for future development. Different model assumptions and erosive controls may be appropriate for either turbulent or more laminar periods of flow. For the recorded flows considered here, the concentration data were of insufficient time resolution to be able to calculate a robust Reynolds number data set throughout the flow. However, if future studies are able to collect accurate, high-resolution, time-dependent fluid densities, in addition to flow velocity and stage, then the calculation of the Reynolds number may provide a quantitative determination of the transition between laminar and turbulent flow (Waltham, 2004). This would provide a useful comparison to seismic and visual data, while also aiding descriptions of the relationship between flow rheology and the dominance of erosion and sedimentation.

A lahar can appear to bulk locally, if its total length shortens due to channel conditions, or as faster moving packets migrate toward the flow front, causing the total lahar to shorten and individual packets to coalesce. True bulking can only be determined by calculating the discharge difference between sites. From these data we have been able to identify distinct occurrences of bulking and debulking as the wave passes. Numerical calculations by Fagents and Baloga (2006) suggest that water losses by infiltration are not significant during the passage of the lahar. However, our results indicate that debulking is common at the head of such small, rain-induced flows, most likely due to low discharge (Fig. 7). In addition, water loss may occur via infiltration into an unsaturated permeable substrate (Manville, 2004; Scott et al., 2005; Fagents and Baloga, 2006). While this may only affect the total volume by <7%, it may make the substrate more susceptible to erosion by the later phases of the flow. Thus, the later flow may bulk further by entraining both this sediment and the new pore water.

In conclusion, our results indicate that bulking and debulking can be localized to certain portions of a lahar, with peak discharge changes much greater than the total overall event estimates. Lahars, and portions within them, are shown to bulk when they have a high discharge and debulk when they have a low discharge, changing their discharge and volume greatly. This threshold observation has applications beyond rainfall-induced lahars to all types of debris flows, turbidity currents, flood surges, and industrial slurry flows. For such flows the understanding and quantification of intraevent changes is vital for the development of numerical models used to identify site-specific inundation, avulsion, erosion, and associated hazards.

ACKNOWLEDGMENTS

We gratefully thank Emma Phillips for extensive PIV analysis, Céline Dumaisnil, Yves Bru, the Leng-kong villagers, Mahjum and Latif Usman for field assistance, Kat Holt for further PIV analysis, and Suzy E. Cole for very helpful discussions regarding the seismic data. We also thank the reviewers Chris Newhall, Tom Pierson, and Sarah Fagents for helpful comments that improved our presentation. EED and SJC are supported by the Marsden Fund (MAUX0512) and the New Zealand Foundation for Research, Science, and Technology grant (MAUX0401). JCT thanks the French-Indonesian Volcanisme Explosif Laboratoire Indonésien research and exchange program.

REFERENCES CITED

Arattano, M., and Grattoni, P., 2000, Using a fixed video camera to measure debris-flow surface velocity, *in* Wieczorek, G., and Naeser, N., eds., *Debris-Flow Hazards Mitigation: Rotterdam, Mechanics, Prediction, and Assessment*, p. 273–281.

Arattano, M., and Marchi, L., 2008, Systems and sensors for debris-flow monitoring and warning: *Sensors*, v. 8, p. 2436–2452, doi: 10.3390/s8042436.

Arattano, M., and Moia, F., 1999, Monitoring the propagation of a debris flow along a torrent: *Hydrological Sciences Journal*, v. 44, p. 811–823.

Beverage, J., and Culbertson, J., 1964, Hyperconcentrations of suspended sediment: *American Society of Civil Engineers*, v. 90, p. 117–126.

Buchanan, T.J., and Somers, W.P., 1969, *Techniques of Water-Resources Investigations of the United States Geological Survey, Book 3, Applications of Hydraulics: Discharge measurements at gauging stations: Chapter A8: U.S. Geological Survey*, 2nd edition.

Cao, Z., Pender, G., and Carling, P., 2006, Shallow water hydrodynamic models for hyperconcentrated sediment-laden floods over erodible flood: *Advances in Water Resources*, v. 29, p. 546–557, doi: 10.1016/j.advwatres.2005.06.011.

Capra, L., Macías, J.I., Scott, K.M., Abrams, M., and Garduño-Monroy, V.H., 2002, Debris avalanches and debris flows transformed from collapses in the Trans-Mexican Volcanic Belt, Mexico—Behavior, and implications for hazard assessment: *Journal of Volcanology and Geothermal Research*, v. 113, p. 81–110, doi: 10.1016/S0377-0273(01)00252-9.

Caruso, P., and Pareschi, M.T., 1993, Estimation of lahar and lahar-runout flow hydrograph on natural beds: *Environmental Geology*, v. 22, p. 141–152.

Chen, C., 1987, Comprehensive review of debris flow modeling concepts in Japan: *Reviews in Engineering Geology*, v. 7, p. 13–29.

Chow, V.T., 1959, *Open-Channel Hydraulics*: New York, Toronto, London: McGraw-Hill Civil Engineering Series, McGraw-Hill Book Company.

Cole, S., Cronin, S., Sherburn, S., and Manville, V., 2009, Seismic signals of snow-slurry lahars in motion: 25 September 2007, Mt. Ruapehu, New Zealand: *Geophysical Research Letters*, v. 36, p. L09405, doi: 10.1029/2009GL038030.

Costa, J.E., 1988, Rheologic, geomorphic, and sedimentologic differentiation of water floods, hyperconcentrated flows, and debris flows, *in* Baker, V.R., Kochel, R.C., and Patton, P.C., eds., *Flood Geomorphology*: New York: John Wiley and Sons, p. 113–122.

Coussot, P., 2005, Rheometry of Pastes, Suspensions, and Granular Materials: Applications in Industry and Environment: John Wiley and Sons, 312 p.

Coussot, P., and Meunier, M., 1996, Recognition, classification and mechanical description of debris flows: *Earth-Science Reviews*, v. 40, p. 209–227, doi: 10.1016/0012-8252(95)00065-8.

Creutin, J., Muste, M., Bradley, A., Kim, S., and Kruger, A., 2003, River gauging using PIV techniques: A proof of concept experiment in the Iowa River: *Journal of Hydrology (Amsterdam)*, v. 277, p. 182–194, doi: 10.1016/S0022-1694(03)00081-7.

Cronin, S.J., Neall, V.E., Leconte, J.A., and Palmer, A.S., 1997, Changes in Whangāehu River lahar characteristics during the 1995 eruption sequence, Ruapehu volcano, New Zealand: *Journal of Volcanology and Geothermal Research*, v. 76, p. 47–61, doi: 10.1016/S0377-0273(96)00064-9.

Cronin, S.J., Neall, V.E., Leconte, J.A., and Palmer, A.S., 1999, Dynamic interactions between lahars and stream flow: A case study from Ruapehu volcano, New Zealand: *Geological Society of America Bulletin*, v. 111, p. 28–38, doi: 10.1130/0016-7606(1999)111<0028:DIBLAS>2.3.CO;2.

Cronin, S.J., Leconte, J.A., Palmer, A.S., and Neall, V.E., 2000, Transformation, internal stratification, and deposition of a channelised, multi-peaked lahar flow: *New Zealand Journal of Geology and Geophysics*, v. 43, p. 117–128, doi: 10.1080/00288306.2000.9514874.

Dalziel, S., 2005, Digiflow user guide: <http://www.dampm.cam.ac.uk/lab/digiflow/>.

Doyle, E.E., Cronin, S.J., Cole, S.E., and Thouret, J.-C., 2009, The challenges of incorporating temporal and spatial changes into numerical models of lahars, *in* Anderssen, R.S., Braddock, R.D., and Newham, L.T.H., eds., *Proceedings of the 18th World IMACS Congress and MODSIM09 International Congress on Modelling and Simulation: Modelling and Simulation Society of Australia and New Zealand and International Association for Mathematics and Computers in Simulation*, July 2009, p. 2665–2671.

Doyle, E.E., Cronin, S.J., Cole, S.E., and Thouret, J.C., 2010, The coalescence and organization of lahars at Semeru Volcano, Indonesia: *Bulletin of Volcanology*, doi: 10.1007/s00445-010-0381-8.

Dumaisnil, C., Thouret, J.C., Chambon, G., Doyle, E.E., and Cronin, S.J., 2010, Physical and rheological characteristics of lahar flows and deposits—A case study at Semeru volcano, Java (Indonesia): *Earth Surface Processes and Landforms*, v. 35, doi: 10.1002/esp.2003.

Dyer, K.R., and Soulsby, R.L., 1988, Sand transport on the continental shelf: *Annual Review of Fluid Mechanics*, v. 20, p. 295–324, doi: 10.1146/annurev.fl.20.010188.001455.

Fagents, S.A., and Baloga, S.M., 2006, Toward a model for the bulking and debulking of lahars: *Journal of Geophysical Research*, v. 111, p. B10201, doi: 10.1029/2005JB003986.

Fisher, R.V., and Schmincke, H.U., 1984, *Pyroclastic Rocks*, Chapter 11: Berlin, Heidelberg, New York, Tokyo, Springer-Verlag.

Garcia, M., and Parker, G., 1991, Entrainment of bed sediment into suspension: *Journal of Hydraulic Engineering*, v. 117, p. 414–435, doi: 10.1061/(ASCE)0733-9429(1991)117:4(414).

Hayes, S., Montgomery, D., and Newhall, C., 2002, Fluvial sediment transport and deposition following the 1991 eruption of Mount Pinatubo: *Geomorphology*, v. 45, p. 211–224, doi: 10.1016/S0169-555X(01)00155-6.

Huang, C.J., Shieh, C.L., and Yin, H.Y., 2004, Laboratory study of the underground sound generated by debris flows: *Journal of Geophysical Research*, v. 109, p. F01008, doi: 10.1029/2003JF000048.

Hungr, O., McDougall, S., and Bovis, M., 2005, Entrainment of material by debris flows, *in* Jakob, M., and Hungr, O., eds., *Debris Flow Hazards and Related Phenomena*, Chapter 7: New York, Springer-Verlag, p. 136–157.

Hürlimann, M., Rickenmann, D., and Graf, C., 2003, Field and monitoring data of debris-flow events in the Swiss Alps: *Canadian Geotechnical Journal*, v. 40, p. 161–175, doi: 10.1139/t02-087.

Iverson, R.M., 1997, The physics of debris flows: *Reviews of Geophysics*, v. 35, p. 245–296, doi: 10.1029/97RG00426.

Iverson, R.M., 2005, Debris flow mechanics, *in* Jakob, M., and Hungr, O., eds., *Debris flow hazards and related phenomena*, Chapter 5: New York, Springer-Verlag, p. 105–131.

Iverson, R.M., and Denlinger, R.P., 2001, Flow of variably fluidized granular masses across three-dimensional terrain. 1. Coulomb mixture theory: *Journal of Geophysical Research*, v. 106, p. 537–552, doi: 10.1029/2000JB900329.

Iverson, R.M., Reid, M.E., and LaHusen, R.G., 1997, Debris-flow mobilization from landslides: *Annual*

- Review of Earth and Planetary Sciences, v. 25, p. 85–138, doi: 10.1146/annurev.earth.25.1.85.
- Jakob, M., and Hungr, O., eds., 2005, Debris-flow Hazards and Related Phenomena: New York: Springer-Verlag, p. 136–157.
- Klein, G., Yufit, G., and Shkurko, V., 1993, A new moving boat method for the measurement of discharge in large rivers: *Hydrological Sciences Journal*, v. 38, p. 79–88, doi: 10.1080/02626669309492647.
- Knighton, D., 1998, Fluvial forms and processes: A new perspective: London, Arnold.
- Komar, P.D., 1988, Sediment transport by floods, in *Flood Geomorphology*, Chapter 6: New York, John Wiley and Sons, p. 97–111.
- Lavigne, S., and Suwa, H., 2004, Contrasts between debris flows, hyperconcentrated flows, and stream flows at a channel of Mount Semeru, East Java, Indonesia: *Geomorphology*, v. 61, p. 41–58, doi: 10.1016/j.geomorph.2003.11.005.
- Lavigne, F., and Thouret, J.C., 2002, Sediment transport and deposition by rain-triggered lahars at Merapi volcano, Central Java, Indonesia: *Geomorphology*, v. 49, p. 45–69, doi: 10.1016/S0169-555X(02)00160-5.
- Lavigne, F., Thouret, J.C., Voight, B., Young, K., La Husen, R., Marso, J., Suwa, H., Sumaryono, A., Sayudi, D., and Dejean, M., 2000, Instrumental lahar monitoring at Merapi volcano: *Journal of Volcanology and Geothermal Research*, v. 100, p. 457–478, doi: 10.1016/S0377-0273(00)00151-7.
- Lavigne, F., Tirel, A., Le Froch, D., and Veyrat-Charvillon, S., 2003, A real-time assessment of lahar dynamics and sediment load based on video-camera recording at Semeru Volcano, Indonesia, in Rickenman, D., and Chen, C., eds., *Debris-Flow Hazards Mitigation: Mechanics, Prediction, and Assessment*, v. 2: Rotterdam, Millpress, p. 871–882.
- Lenzi, M.A., and Marchi, L., 2000, Suspended sediment load during floods in a small stream in the dolomites (northeastern Italy): *Catena*, v. 39, p. 267–282, doi: 10.1016/S0341-8162(00)00079-5.
- Leopold, L.B., Wolman, M.G., and Miller, J.P., 1995, Fluvial processes in geomorphology: New York, Dover Publications.
- Macedonio, G., and Pareschi, M., 1992, Numerical simulation of some lahars from Mount St. Helens: *Journal of Volcanology and Geothermal Research*, v. 54, p. 65–80, doi: 10.1016/0377-0273(92)90115-T.
- Major, J.J., 1997, Depositional processes in large-scale debris-flow experiments: *The Journal of Geology*, v. 105, p. 345–366, doi: 10.1086/515930.
- Manville, V., 2004, Paleohydraulic analysis of the 1953 Tangiwai lahar: New Zealand's worst volcanic disaster: *Acta Vulcanologica*, v. 16, p. 137–152.
- Manville, V.R., and White, J.D.L., 2003, Incipient granular mass flows at the base of sediment-laden floods, and the roles of flow competence and flow capacity in the deposition of stratified bouldery sands: *Sedimentary Geology*, v. 155, p. 157–173, doi: 10.1016/S0037-0738(02)00294-4.
- Manville, V.R., Cronin, S.J., and members of the Crater Lake Research Team, 2007, Breakout lahar from New Zealand's crater lake: Eos (Transactions, American Geophysical Union), v. 88, no. 43, p. 441–456, doi: 10.1029/2007EO430001.
- Marchi, L., Arattano, M., and Deganutti, A.M., 2002, Ten years of debris-flow monitoring in the Moscardo Torrent (Italian Alps): *Geomorphology*, v. 46, p. 1–17, doi: 10.1016/S0169-555X(01)00162-3.
- Marcial, S., Melosantos, A.A., Hadley, K.C., LaHusen, R.G., and Marso, J.N., 1996, Instrumental lahar monitoring at Mt. Pinatubo, in Newhall, C.G., and Punongbayan, R.S., eds., *Fire and Mud: Eruptions and Lahars of Mount Pinatubo, Philippines*: Seattle, PHIVOLCS and University of Washington Press, p. 1015–1022.
- Massimo, A., 2000, On debris flow front evolution along a torrent: *Physics and Chemistry of the Earth (B)*, v. 25, no. 9, p. 733–740.
- Matthes, G., 1956, River surveys in unmapped territory: *American Society of Civil Engineers*, v. 121, p. 739–758.
- Okuda, S., Suwa, K., Okunishi, K., Yokoyama, K., Ogawa, K., and Hamana, S., 1979, Synthetic observation of debris flows (part 5): *Annuals of Disaster Prevention Research Institute, Kyoto University*, v. 22, p. 175–204 (in Japanese with English abstract).
- Petts, G.E., Foulger, T.R., Gilvear, D.J., Pratts, J.D., and Thoms, M.C., 1985, Wave-movement and water-quality variations during a controlled release from Kielder reservoir, North Tyne river, U.K: *Amsterdam, Journal of Hydrology*, v. 80, p. 371–389, doi: 10.1016/0022-1694(85)90129-5.
- Pierson, T.C., 1995, Flow characteristics of large eruption-triggered debris flows at snow-clad volcanoes: Constraints for debris-flow models: *Journal of Volcanology and Geothermal Research*, v. 66, p. 283–294, doi: 10.1016/0377-0273(94)00070-W.
- Pierson, T.C., 2005, Hyperconcentrated flow transition process between water flow and debris flow, in Jakob, M., and Hungr, O., eds., *Debris flow hazards and related phenomena*, Chapter 8: New York, Springer-Verlag, p. 159–196.
- Pierson, T.C., and Costa, J.E., 1987, A rheological classification of subaerial sediment-water flows, in Costa, J.E., and Wieczorek, G.F., eds., *Debris flows/avalanches—Process, recognition, and mitigation: Reviews in Engineering Geology*, v. 7, p. 1–12.
- Pierson, T.C., and Scott, K.M., 1985, Downstream dilution of a lahar, transition from debris flow to hyperconcentrated streamflow: *Water Resources Research*, v. 21, p. 1511–1524, doi: 10.1029/WR021i010p01511.
- Pierson, T.C., Janda, R.J., Thouret, J.C., and Borrero, C.A., 1990, Perturbation and melting of snow and ice by the 13 November 1985 eruption of Nevado del Ruiz, Colombia, and consequent mobilization, flow, and deposition of lahars: *Journal of Volcanology and Geothermal Research*, v. 41, p. 17–66, doi: 10.1016/0377-0273(90)90082-Q.
- Pritchard, D., 2005, On fine sediment transport by a flood surge: *Journal of Fluid Mechanics*, v. 543, p. 239–248, doi: 10.1017/S0022112005006518.
- Pritchard, D., and Hogg, A., 2002, On sediment transport under dam-break flow: *Journal of Fluid Mechanics*, v. 473, p. 265–274, doi: 10.1017/S0022112002002550.
- Procter, J., Cronin, S.J., Fuller, I.C., Lube, G., and Manville, V., 2010, Quantifying the geomorphic impacts of a lake-breakout lahar, Mount Ruapehu, New Zealand: *Geology*, v. 38, no. 1, p. 67–70, doi: 10.1130/G30129.1.
- Scott, K.M., 1988, Origins, behavior, and sedimentology of lahars and lahar-runout flows in the Toutle-Cowlitz River system: *U.S. Geological Survey Professional Paper 1447-A*, 74 p.
- Scott, K.M., Vallance, J.W., and Pringle, P., 1995, Sedimentology, behavior, and hazards of debris flows at Mount Rainier, Washington: *U.S. Geological Survey Professional Paper 1547*, 56 p.
- Scott, K.M., Vallance, J.W., Kerle, N., Macias, J.L., Strauch, W., and Devoli, G., 2005, Catastrophic precipitation-triggered lahar at Casita volcano, Nicaragua: Occurrence, bulking, and transformation: *Earth Surface Processes and Landforms*, v. 30, p. 59–79, doi: 10.1002/esp.1127.
- Smith, G.A., 1986, Coarse-grained non-marine volcanoclastic sediment, terminology, and depositional process: *Geological Society of America Bulletin*, v. 97, p. 1–10, doi: 10.1130/0016-7606(1986)97<1:CNVSTA>2.0.CO;2.
- Smith, G.A., and Fritz, W.J., 1989, Volcanic influences on terrestrial sedimentation: *Geology*, v. 17, p. 375–376, doi: 10.1130/0091-7613(1989)017<0375:VIOTS>2.3.CO;2.
- Suwa, H., Yamakoshi, T., and Sato, K., 2000, Relationship between debris-flow discharge and ground vibration, in Wieczorek, G., and Naeser, N., eds., *Debris-Flow Hazards Mitigation: Rotterdam, Mechanics, Prediction, and Assessment*, p. 311–318.
- Takahashi, T., 1991, Debris flow: Rotterdam, A.A. Balkema, International Association of Hydro-Environment Engineering and Research (IAHR) Monograph Series, Taylor and Francis.
- Takahashi, T., ed., 2007, Debris flow: Mechanics, Prediction, and Countermeasures: London, Taylor and Francis.
- Thouret, J.-C., Abdurachman, K.E., Boudier, J.-L., and Bronto, S., 1998, Origin, characteristics, and behavior of lahars following the 1990 eruption of Kelud volcano, eastern Java (Indonesia): *Bulletin of Volcanology*, v. 59, p. 460–480, doi: 10.1007/s004450050204.
- Thouret, J.-C., Lavigne, F., Suwa, H., Sukatja, B., and Suroso, 2007, Volcanic hazards at Mount Semeru, East Java (Indonesia), with emphasis on lahars: *Bulletin of Volcanology*, v. 70, p. 221–244, doi: 10.1007/s00445-007-0133-6.
- Tuñol, N.M., and Regalado, M.T., 1996, Rainfall, acoustic, flow monitor records, and observed lahars of the Sacobia River in 1992, in Newhall, C.G., and Punongbayan, R.S., eds., *Fire and Mud: Eruptions and Lahars of Mount Pinatubo, Philippines*: PHIVOLCS and University of Washington Press, p. 1023–1032.
- Vallance, J.W., 2000, Lahars, in Sigurdsson, H., Houghton, B., McNutt, S.R., Rymer, H., and Stix, J., eds., *Encyclopedia of Volcanoes*: New York, Academic Press, p. 601–616.
- Vignaux, M., and Weir, G., 1990, A general model for Mount Ruapehu lahars: *Bulletin of Volcanology*, v. 52, p. 381–390, doi: 10.1007/BF00302050.
- Waltham, D., 2004, Flow transformations in particulate gravity currents: *Journal of Sedimentary Research*, v. 74, p. 129–134, doi: 10.1306/062303740129.
- Witham, C., 2005, Volcanic disasters and incidents: A new database: *Journal of Volcanology and Geothermal Research*, v. 148, p. 191–233, doi: 10.1016/j.jvolgeores.2005.04.017.
- Xu, J., 2002, Erosion caused by hyperconcentrated flow on the Loess Plateau of China: *Catena*, v. 49, p. 289–307, doi: 10.1016/S0341-8162(02)00064-4.
- Zanuttigh, B., and Lamberti, A., 2007, Instability and surge development in debris flows: *Reviews of Geophysics*, v. 45, p. RG3006, doi: 10.1029/2005RG000175.